DIAGNOSIS OF PUSHER–FUEL MIX IN INDIRECTLY DRIVEN NOVA IMPLOSIONS (HEP3)

T. R. Dittrich
B. A. Hammel
C. J. Keane
R. McEachern
R. E. Turner
S. W. Haan
L. J. Suter

Introduction

A key issue for inertial confinement fusion (ICF) is the hydrodynamic stability of the imploding capsule. Imperfections on the capsule surface can grow into large perturbations that degrade capsule performance. Understanding this process is crucial if we are to successfully predict requirements for future high-gain ICF capsules. Experiments on the Nova laser at Lawrence Livermore National Laboratory have directly measured perturbation growth on planar foils,[1] and three experimental groups have investigated backlit perturbation growth using imploding spheres.[2–4] In addition to these efforts, which concentrate on indirectly driven implosions, is work investigating the hydrodynamic stability of directly driven ICF capsules.[5,6] In these direct-drive experiments the laser light shines directly on the capsules, causing the implosion and providing the seed for perturbation growth.

This article reports measurement, via emission from spectroscopic tracers,[7] of the full process of perturbation growth leading to pusher–fuel mix in spherical implosions, and shows perturbation growth dependence on initial perturbation amplitude and wavelength. In contrast to the cited direct-drive work, we have in this experiment separated the drive from the perturbation seed. (For a review of x-ray spectroscopy of ICF plasmas see Refs. 8 and 9.)

The purpose of the experiments described here was to study, in a controlled manner, the effects of the Rayleigh–Taylor (RT) instability on capsule implosion performance. The mechanism by which RT growth degrades capsule performance can be summarized as follows: As the ablation phase of the implosion proceeds, surface imperfections grow via the RT instability as low-density ablated material pushes on the high-density shell. This growth causes the imploding shock to deviate from spherical, carrying the perturbation information through the shell and rippling the interface between pusher and fuel. When the fuel is compressed later in time, the pusher–fuel interface becomes RT unstable, which causes this rippling to grow and produce a region of mixed pusher and fuel material. Increasing the initial outer surface perturbation increases the degree of pusher–fuel mixing.

Experiment

These Nova experiments use plastic-shelled capsules filled with deuterium (D_2). A typical capsule shell in the experiment had a 420-μm inside diameter and a 55-μm-thick wall, and consisted of three layers. The inner layer, the pusher, was ~3 μm of polystyrene doped with 1.0% (atomic) Cl. The middle layer was a 3-μm-thick permeation barrier made of polyvinylalcohol (PVA), which sealed in the fuel gas. An outer layer of plasma polymer ($CH_{1.3}$) was deposited over the inner layers,[10] forming the ablator. The capsules were filled with 50 atm D_2 gas and 0.1 atm Ar.

The Nova laser indirectly drove the implosion of these capsules. A square pulse of laser light with a duration of 1 ns heated a cylindrical gold case, or *hohlraum*, with (typically) 17 kJ of laser energy. The hohlraum, reaching a peak radiation temperature of 230 eV, then emitted x rays that ablated the plastic and caused the implosion.

The capsules had relatively low convergence (~8) and had considerably less sensitivity to growth of surface perturbations compared to that predicted for current high-gain ICF capsule designs. We chose capsule implosions with low convergence so that asymmetries in the x-ray drive would have little effect on the implosions and would, therefore, not complicate the perturbation growth effects.

To make capsules with various degrees of surface roughness, many polystyrene beads, ranging in diameter from 0.6 to 7 μm, were embedded in the PVA layer. When the ablator layer was deposited onto this rough PVA surface, the perturbations were imprinted on the

outer surface. This method of using a capsule with a controllably rough outer surface as seed for RT growth during implosion contrasts with the method used in Refs. 5 and 6, where direct-drive laser illumination nonuniformity was assumed to be the dominant source of initial amplitude seeds to the RT instability and to be representable by a semi-empirical analytic expression.

After shooting these capsules, we developed the capability of characterizing shell surfaces using an equatorially tracing atomic force microscope (AFM). Using this AFM, we took equatorial traces of capsules from the same production runs as capsules that were shot. (To verify surface similarity, we compared scanning electron microscope images of these traced capsules with images of the shot capsules.) We converted the equatorial traces to power spectra and combined them to form ensemble averages. By assuming that the surface bumpiness is isotropic, we transformed these one-dimensional (1-D) average power spectra into 2-D (spherical surface) power spectra:[11]

$$P_{2D}(l) = \left(l + \frac{1}{2}\right) \sum_{n=l,\,l+2}^{\infty} \left[P_{1D}(n) - P_{1D}(n+2)\right] \times \frac{(n+l)!!\,(n-l-1)!!}{(n-l)!!\,(n+l+1)!!} \qquad (1)$$

where l is the perturbation mode number, P_{1D} is the 1-D power spectrum and P_{2D} is the 2-D power spectrum. Figure 1 shows 2-D (spherical surface) power spectra of capsules with rms = 0.03, 0.31, and 1.75 μm.

We diagnosed enhanced pusher–fuel mix due to these surface perturbations in two ways. First, we monitored the variation in capsule DD neutron yield with roughness; this we expected to decrease with increasing surface roughness as cold dense pusher material increasingly poisoned the fuel. Second, we monitored the variation in the x-ray self-emission of included trace elements, or dopants,[7,12] with roughness. We expected the x-ray emission of the pusher dopant, Cl, to increase relative to the x-ray emission of the fuel dopant, Ar, as the surface roughness was increased. In the temperature and density regime accessed in these experiments, the variation of x-ray line radiation from these dopants depends strongly on temperature. During the implosion, PdV work heated the fuel and the Ar, but conduction and convection, due to mix, heated the Cl. At peak x-ray emission the imploded capsule had steep gradients through the mix region in both electron temperature and density as a function of radius. This made a simple one-temperature, 1-D understanding of this process difficult. We therefore observed the x-ray emission by means of a crystal spectrometer coupled to an x-ray streak camera, which had temporal resolution of ~30 ps and a spectral resolving power ($\lambda/\delta\lambda$) ~700.[13]

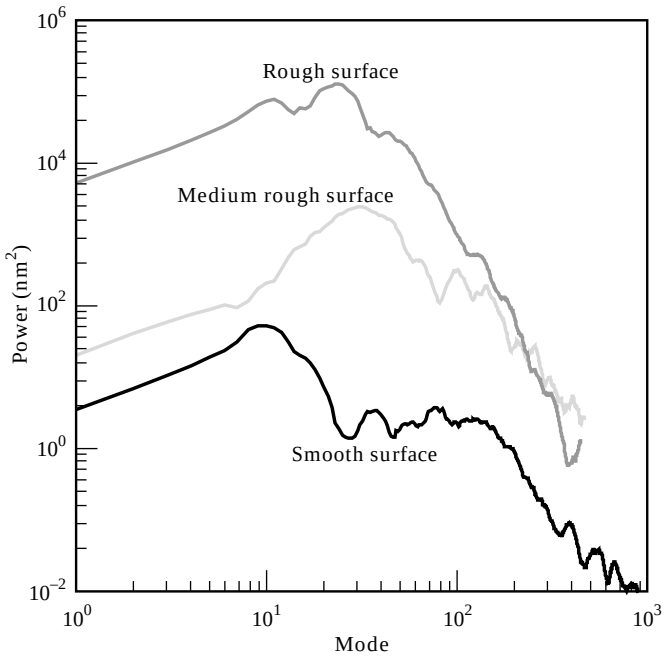

FIGURE 1. The 2-D (spherical surface) power spectra characterizing the outer surface of three representative capsules with rms = 0.03, 0.31, and 1.70 μm. (20-03-0795-1848pb01)

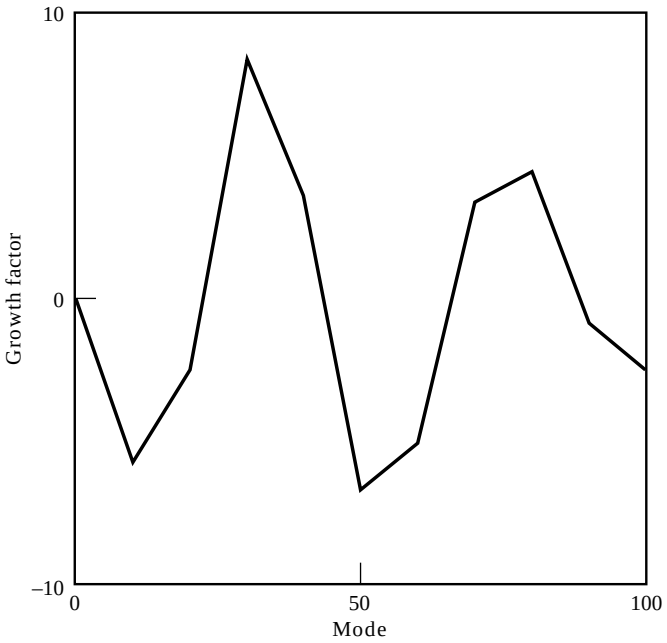

FIGURE 2. Growth factor at pusher–fuel interface vs mode number for perturbations initially on the capsule outer surface. This is a snapshot at time of peak neutron production. Negative values indicate phase change of the perturbation. (20-03-0795-1849pb01)

Analysis Method

Simulating the implosion of these capsules was a multistep process. First, we estimated the capsule's sensitivity to surface perturbations. Second, we combined the surface roughness with the perturbation growth factors. Third, we ran implosion simulations to generate emission spectra. This section describes the three steps.

First, we estimated the capsule's sensitivity to surface perturbations using several 2-D LASNEX[14] simulations, from which we estimated linear growth for several single modes. The initial perturbations in these simulations were small to ensure that only linear growth would occur. This perturbation growth included the effects of stabilization at the ablation surface, feed-through between the interfaces, and RT / Richtmyer–Meshkov instability growth at the pusher–fuel interface. Figure 2 plots these linear growth factors at the pusher–fuel interface vs perturbation mode number. This growth factor is the amplification of a perturbation initially on the outer surface as it imprints on the inner capsule surface. It is typically quoted at peak neutron emission. Negative growth factor values indicate phase change of the perturbation. This linear perturbation growth is small relative to high-gain ICF capsules because of favorable stabilization mechanisms at the ablation surface.

Next, we combined the surface roughness, $P_{2D}(l)$, with the linear perturbation growth factors per standard linear analysis. We estimated nonlinear saturation with Haan's criterion,[15] which states that saturation occurs on a spherical surface of radius R when amplitudes become larger than $4R/l^2$. These saturated amplitudes then grow at a constant rate, rather than exponentially. This procedure predicted the pusher–fuel mixing vs time, estimated from the calculated rms deviation, σ, of the pusher–fuel surface from spherical. The limit of the bubble tips outward was taken to be $\sqrt{2}\sigma$, and the extent of spike tips inward to be $(1+A)\sqrt{2}\sigma$, where A is the Atwood number. This mix-region size estimate also included contributions from both initial pusher–fuel surface imperfections and effects of embedding microspheres in the PVA layer of some of the capsules. Atomic mixing of the pusher and fuel was assumed throughout the mixed region. This modeling distributed the materials within this region so as to maintain a constant concentration while conserving individual material amounts.

Finally, LASNEX implosion simulations used this time-dependent mix region in a self-consistent manner (i.e., the mixing affected the hydrodynamic evolution) and generated emission spectra by means of Detailed Configuration Accounting (DCA).[16,17] These 1-D simulations used detailed atomic models for both Ar and Cl. The DCA simulated spectra were calculated using 69- and 70-level atomic models for Cl and Ar, respectively. We produced the models with the DSP[18] code, which contains atomic physics identical to that used in the RATION code.[19]

TABLE 1. Nova shots in the Ar / Cl implosion series.

Shot	Imbedded bead diameter (μm)	Surface rms (μm)	Observed yield (10^9 neutrons)	Observed yield / clean (no mix) yield
1	None	0.031	1.21	0.72
2	None	0.031	1.26	0.83
3	None	0.064	0.53	0.33
4	None	0.065	1.01	0.60
5	0.6	0.307	0.60	0.35
6	2.0	0.308	1.22	0.49
7	2.0	0.308	0.65	0.44
8	3.9–7.0	1.70	0.66	0.20
9	3.9–7.0	1.70	0.70	0.20

Data Analysis

Table 1 lists capsule surface conditions and observed and simulated yields for the nine Nova shots that comprise this experimental series. We have chosen three of these shots to illustrate the variation in x-ray spectral output during implosion with initial capsule surface roughness.

Figure 3 shows spectra at peak x-ray emission for the implosion of a smooth (0.03-μm-rms) capsule. Figure 3(a) shows the spectrum observed with the spectrometer and Fig. 3(b) shows the analogous DCA simulated spectrum. Very little Cl Ly-α emission, relative to Ar Ly-α, is evident in either of these spectra. The simulations indicate that 6% of the total Cl mass has reached at least 600 eV. The simulated Ly-α satellite line strengths, on the low-energy side of the Ly-α lines, differ from those observed; the large absorption feature evident in Fig. 3(b) at 2.75–2.80 keV is probably due to errors in calculating the opacity of the Cl He-α line in the colder plastic away from the pusher–fuel interface. Figure 4 shows the spectra from an intermediately rough (0.31-μm-rms) capsule. In this case the Ly-α emissions from both the Cl and Ar are comparable in strength, and 10% of the total Cl mass (according to simulation) has reached at least 600 eV. Figure 5 shows the spectra from a very rough (1.75-μm-rms) capsule. In this case the Cl Ly-α emission is stronger than the Ar Ly-α emission, and 15% of the total Cl mass (according to simulation) has reached at least 600 eV. The simulations show that from smooth to rough capsules the Cl Ly-α emission increased by 350% but the Ar Ly-α emission decreased by 30%.

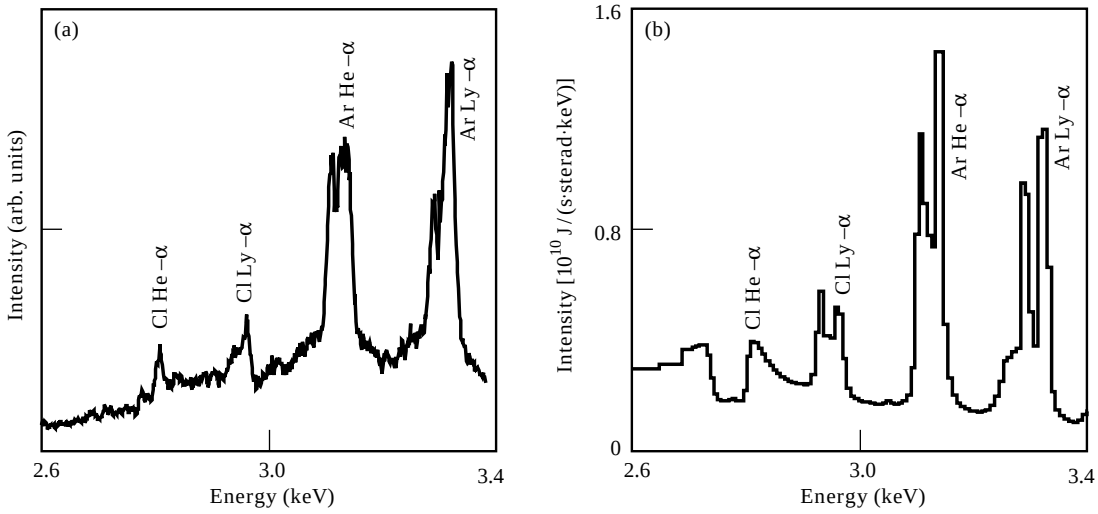

FIGURE 3. Spectra at peak x-ray emission from the implosion of a smooth surface (rms = 0.03 μm) capsule. (a) is as observed by the streaked crystal spectrometer. (b) is the 1-D DCA simulation of this shot. Relevant emission lines of Cl and Ar are labeled.
(20-03-0795-1850pb02)

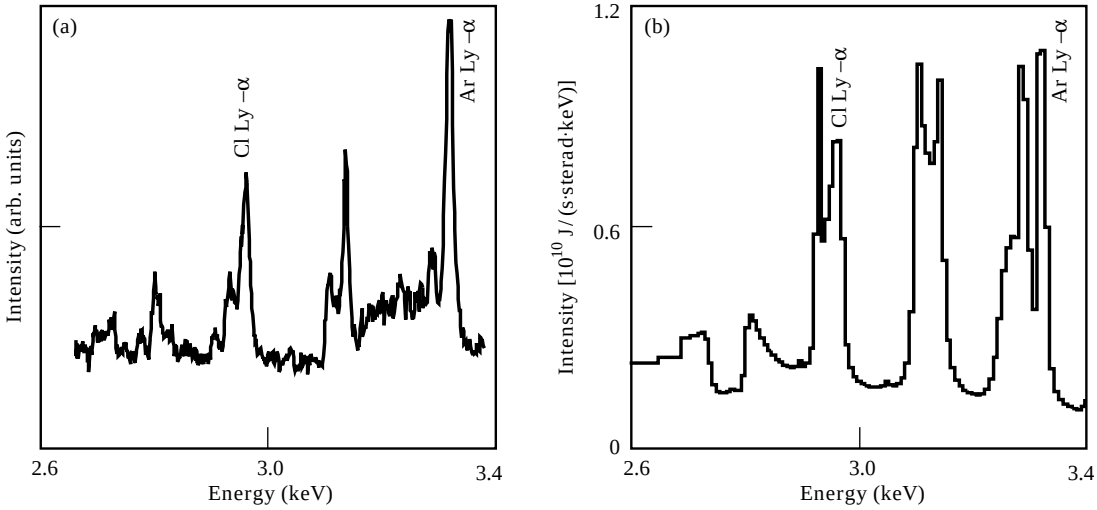

FIGURE 4. Same as Fig. 3, for an intermediate roughness (rms = 0.3 μm) capsule.
(20-03-0795-1851pb02)

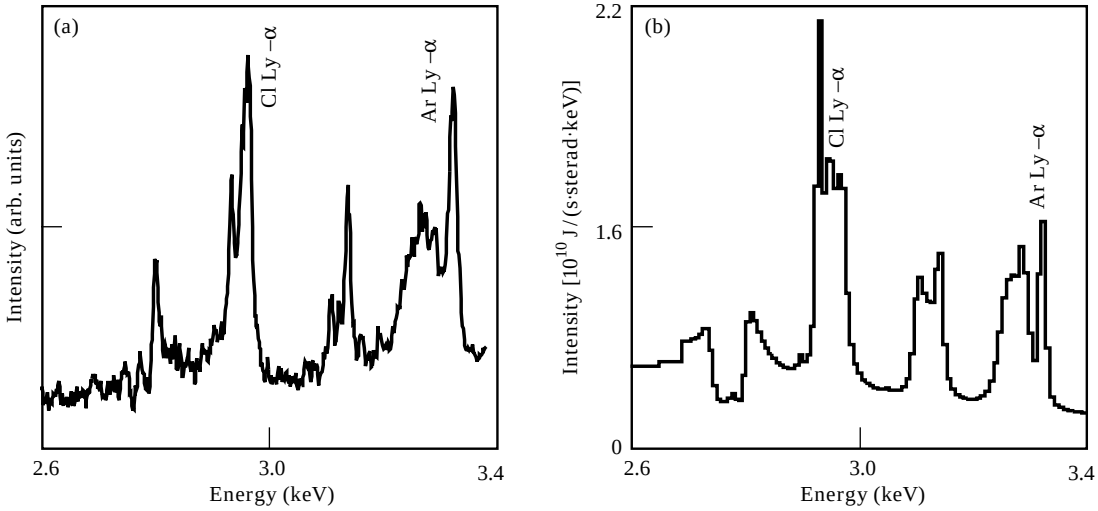

FIGURE 5. Same as Fig. 3, for a very rough (rms = 1.7 μm) capsule.
(20-03-0795-1852pb02)

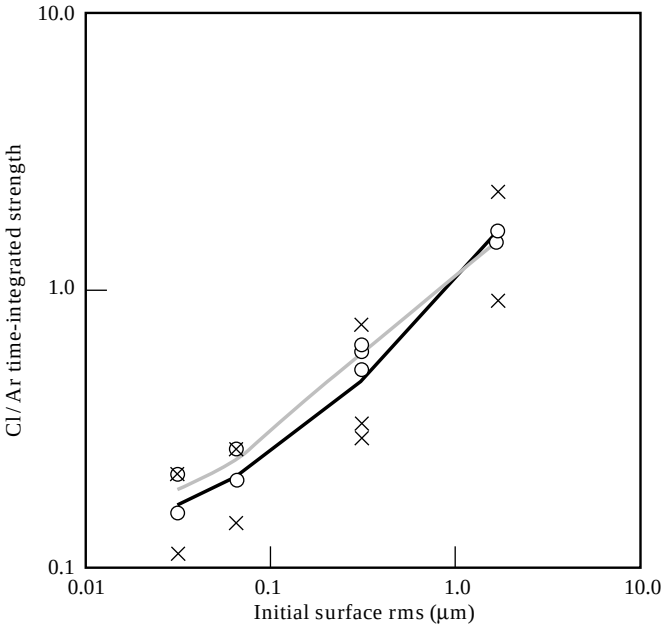

FIGURE 6. Comparison of simulated and observed emission spectra from the nine shots in the series. The ratio of time-integrated Cl and Ar Ly-α emission is plotted vs surface finish. X marks experimental points; O marks simulation points. The black and gray lines are the results of averaging the experimental and simulation values, respectively, at each distinct rms value. (20-03-0795-1853pb01)

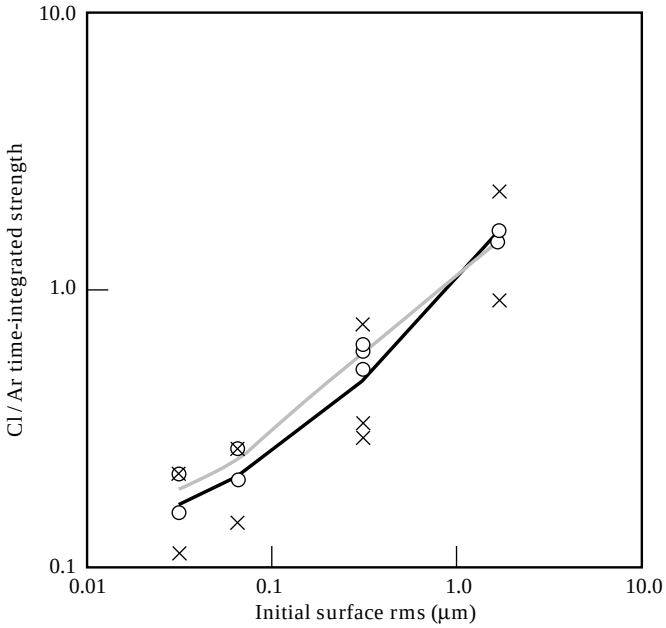

FIGURE 7. Observed and simulated mixed neutron yield over clean yield, vs surface finish for the same nine-shot data set. The black and gray lines are the results of averaging the experimental and simulation values, respectively, at each distinct rms value. (20-03-0795-1854pb01)

To quantitatively compare the observed and simulated spectra, we ratio the time-integrated Ly-α emission from the two dopants. (At each time we estimated this line emission by subtracting the continuum and background and deconvolving the result into distinct Gaussian-shaped peaks. In this manner we eliminated contributions from the strong satellite lines of the Ly-α transitions and the Cl He-β line at 3.27 keV.) The Ar Ly-α strength effectively normalizes the Cl Ly-α strength to the specifics of capsule performance such as capsule size, laser drive, and diagnostic calibration.

Figure 6 shows this comparison of observed and simulated emission spectra by means of the ratio of time-integrated Ly-α lines for all nine shots. The ratio of emission strength smoothly changed a factor of ~9 for a surface rms change of ~50. Figure 7 shows observed and simulated mixed neutron yield over clean yield vs rms surface finish for the same nine-shot data set.

To test the importance of the saturation modeling, we also estimated the perturbation growth with unmodified linear analysis. The modification due to saturation is quite small, and given the large spread in experimental results, no conclusion can be made regarding the correctness of the saturation modeling procedure.

Conclusion

Both the observed x-ray emission and neutron yield from the 1-ns-drive Nova implosions show significant variation as a function of initial capsule surface finish. Furthermore, we can successfully interpret this variation as a dependence of pusher–fuel mix on initial surface roughness. This interpretation derives from modeling based on linear analysis using multiple 2-D LASNEX simulations and 1-D mixed implosion modeling using LASNEX and DCA to simulate neutron output and x-ray emission of included dopants.

Acknowledgments

The authors wish to thank Craig Moore for his efforts in capsule characterization, Ravi Upadhye and Blanca Haendler for their early work in rough-surfaced capsule fabrication, and Steve Langer, Steve Hatchett, and Yim Lee for assistance in simulation details.

Notes and References

1. B. A. Remington, S. V. Weber, S. W. Haan, J. D. Kilkenny, et al., *Phys. Fluids B* 5, 2589–2595 (1993).
2. J. S. Wark, J. D. Kilkenny, A. J. Cole, M. H. Key, and P. T. Rumsby, *Appl. Phys. Lett*. 48, 969–971 (1986).
3. H. Nishimura, H. Takabe, K. Mima, F. Hattori, et al., *Phys. Fluids* 31, 2875–2883 (1988).
4. W. Mead, A. Hauer, Los Alamos National Laboratory, Los Alamos, NM, private communication, 1988.
5. D. K. Bradley, J. A. Delettrez, and C. P. Verdon, *Phys. Rev. Lett.* 68, 2774–2777 (1992).
6. J. Delettrez, D. K. Bradley, P. A. Jaanimagi, and C. P. Verdon, *Phys. Rev. A* 41, 5583–5593 (1990).
7. B. A. Hammel, C. J. Keane, T. R. Dittrich, D. R. Kania, et al., *J. Quant. Spectrosc. Radiat. Transfer* 51, 113–124, (1994).
8. A. A. Hauer, N. D. Delamater, and Z. M. Koenig, *Laser and Particle Beams* 9, 3–48 (1991).
9. C. J. Keane, B. A. Hammel, D. R. Kania, J. D. Kilkenny, et al., *Phys. Fluids B* 5, 3328–3336 (1993).
10. S. A. Letts, D. W. Meyers, and L. A. Witt, *J. Vac. Sci. Technol.* 19, 739–742 (1981).
11. S. Pollaine, S. P. Hatchett, S. H. Langer, *ICF Quarterly Report* 4(3), 87–89, Lawrence Livermore National Laboratory, Livermore, CA, UCRL-LR-105820-94-3 (1994).
12. B. A. Hammel, C. J. Keane, M. D. Cable, D. R. Kania, et al., *Phys. Rev. Lett*. 70, 1263–1266 (1993).
13. B. A. Hammel, P. Bell, C. J. Keane, R. W. Lee, *Rev. Sci. Instrum*. 61, 2774–2776 (1990).
14. G. B. Zimmerman, W. L. Kruer, *Comments on Plasma Physics and Controlled Fusion* 2, 51–61 (1975).
15. S. W. Haan, *Phys. Rev. A* 39, 5812 (1989).
16. Y. T. Lee, D. S. Bailey, and G. B. Zimmerman, *Laser Program Annual Report 1985*, UCRL-50021-85, 2.81–2.86 (1985).
17. Y. T. Lee, *J. Quant. Spectrosc. Radiat. Transfer* 38, 131–145 (1987).
18. C. J. Keane, R. W. Lee, and J. P. Grandy, in *Proceedings of the 4th International Workshop on the Radiative Properties of Hot Dense Matter*, Eds., W. Goldstein, C. Hooper, J. Gauthier, J. Seely, and R. W. Lee (World Scientific, Singapore, 1991), p. 233.
19. R. W. Lee, B. L. Whitten, and J. E. Strout, III, *J. Quant. Spectrosc. Radiat. Transfer* 32, 91 (1984).